International Journal of Minerals, Metallurgy and Materials
Volume 20, Number 6, June 2013, Page 529
DOI: 10.1007/s12613-013-0761-0

Hot compression deformation behavior of AISI 321 austenitic stainless steel

Mehdi Haj[1)], *Hojjatollah Mansouri*[1)], *Reza Vafaei*[1)], *Golam Reza Ebrahimi*[2)], *and Ali Kanani*[1)]

1) Department of Materials Engineering, Malek Ashtar University of Technology, Isfahan, Shahin-shahr 83145-115, Iran

2) Department of Materials and Polymer Engineering, Faculty of Engineering, Hakim Sabzevari University, Sabzevar 9617976487, Iran

(Received: 30 July 2012; revised: 6 September 2012; accepted: 11 September 2012)

Abstract: The hot compression behavior of AISI 321 austenitic stainless steel was studied at the temperatures of 950-1100°C and the strain rates of 0.01-1 s^{-1} using a Baehr DIL-805 deformation dilatometer. The hot deformation equations and the relationship between hot deformation parameters were obtained. It is found that strain rate and deformation temperature significantly influence the flow stress behavior of the steel. The work hardening rate and the peak value of flow stress increase with the decrease of deformation temperature and the increase of strain rate. In addition, the activation energy of deformation (Q) is calculated as 433.343 kJ/mol. The microstructural evolution during deformation indicates that, at the temperature of 950°C and the strain rate of 0.01 s^{-1}, small circle-like precipitates form along grain boundaries; but at the temperatures above 950°C, the dissolution of such precipitates occurs. Energy-dispersive X-ray analyses indicate that the precipitates are complex carbides of Cr, Fe, Mn, Ni, and Ti.

Keywords: austenitic stainless steel; deformation; constitutive equations; microstructural evolution; activation energy

1. Introduction

AISI 321 austenitic stainless steel stabilized by titanium has good mechanical properties and corrosion resistance, and is widely used in the power generation industries. This steel is also used in the super heater tubing in conventional coal-fired boilers and other critical applications, such as tubes, pipes, and pressure vessels in gas-cooled nuclear reactors [1].

Titanium combines with carbon and nitrogen to form carbonitrides in this type of steel. This reduces the susceptibility of intergranular stress corrosion cracking through reducing the chromium carbide precipitation along grain boundaries. Also as a solute in the matrix, titanium can significantly retard the recrystallization and grain growth during hot rolling operations [2-6].

Despite the extensive works were carried out on some aspects of AISI 321 stainless steel [2-9], but only a very few study was reported on the high-temperature deformation of this steel [10-12]. Therefore, the aim of this investigation was to evaluate the hot deformation behavior of AISI 321 stainless steel and optimize the hot working processes by analyzing the microstructural evolution. Moreover, the appropriate constitutive equations and the relationship between hot deformation parameters were considered to calculate the flow stress behavior of the steel during deformation.

2. Material and methods

The chemical composition of AISI 321austenitic stainless steel used in this investigation is given in Table 1.

Table 1. Chemical composition of AISI 321 austenitic stainless steel **wt%**

C	Cr	Ni	Mn	Cu	Si	Ti	Mo	W	Al	V	P	S
0.056	18.91	11.19	1.28	0.15	0.79	0.48	0.17	0.07	0.055	0.05	0.025	0.007

Corresponding author: Mehdi Haj E-mail: mehdihaj2003@gmail.com

Cylindrical specimens, with the diameter and height of 5 and 10 mm, respectively, were prepared with their axes aligned along the rolling direction. To minimize the occurrence of inhomogeneous compression due to the friction between specimens and anvils, glass plates were put into graves as a lubricant [13-14].

The single-hit hot compression tests were carried out using a dilatometer machine equipped with the induction furnace and vacuum chamber. All the samples were reheated to 1150°C and held for 10 min, then subjected to the continuous hot compression tests at the temperatures of 950, 1000, 1050, and 1100°C. The strain rates were set as 0.01, 0.1, and 1 s^{-1}, and the strain was taken as 0.9 for all conditions in the measuring data recorder of the dilatometer. This smart equipment did the hot deformation procedure automatically according to the needed force to deform the specimens and the failure tolerance of Al_2O_3 anvils.

A thermocouple was attached to samples to measure the testing temperature directly. After each deformation test, the samples were quenched in the argon gas. Metallographic preparation of samples was carried out using the standard polishing procedure along the longitudinal axis of samples, and etched electrochemically in a solution of 10wt% oxalic acid. To follow the microstructural changes during hot deformation, the microstructures of samples were characterized using both optical microscopy and scanning electron microscopy (SEM). The method by Ebrahimi and Najafizadeh [15] was used to minimize the effect of friction on stress-strain curves.

3. Results and discussion

3.1. True stress-strain curves of AISI 321 stainless steel

Fig. 1 shows the true stress-strain curves obtained at various deformation temperatures and strain rates. It is evident that the peak stresses increase with the increase in strain rate and the decrease in temperature (increasing Zener-Hollomon parameter), and the deformation amount in some conditions is less than 0.9. In hot deformation processes, such as hot compression, many experimental dynamic recrystallization (DRX) flow curves are incomplete. In some deformation conditions, the steady-state strain is high, and reaching to the higher strains is difficult [16].

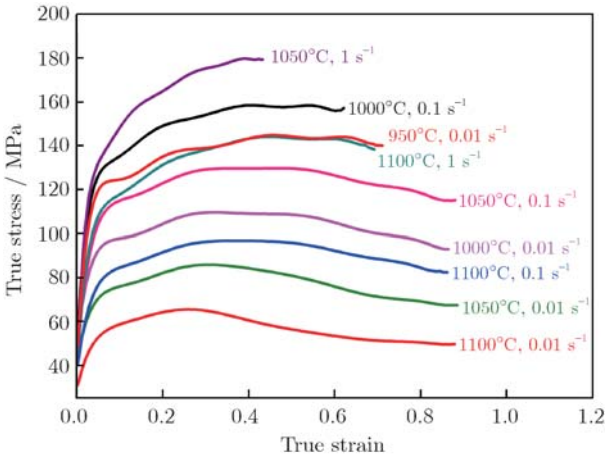

Fig. 1. True stress-true strain curves attained from hot compression test.

At temperatures above 1000°C, most flow curves exhibit a peak stress followed by a slow continuous decrease to a steady level due to the occurrence of DRX. When the specimens deform at a strain rate of 1 s^{-1} and the temperatures of 1050 and 1100°C, the flow curves exhibit a steady flow after the initial work hardening with no signs of DRX, but the occurrence of DRX is traditionally identified from the presence of stress peaks in flow curves. However, not all materials display the well-defined peaks under the hot working conditions. Najafizadeh *et al.* [17] and Poliak *et al.* [12] showed that the onset of DRX could be detected from the inflections in plots of strain hardening rate vs. stress. Therefore, this technique requires the differentiation of stress-strain curves [14, 17].

Deformation at 950°C and a strain rate of 0.01 s^{-1} produces a wavy appearance on the flow curve, which is more pronounced at the beginning of flow. The reason for this may be the occurrence of discontinuous softening due to the presence of more precipitates at this temperature [18-19].

3.2. Constitutive equations of flow stress for AISI 321 stainless steel

Constitutive equations are used to calculate the flow stress of materials during deformation. The base equation is generally determined by Zener-Hollomon parameter (Z), expressing the relationship of stress (σ), temperature (T), and strain rate ($\dot{\varepsilon}$) as [20-21]

$$Z = \dot{\varepsilon} \exp\left(\frac{Q}{RT}\right) = f(\sigma) \tag{1}$$

$$f(\sigma) = \begin{cases} A'\sigma^{n'} & \alpha\sigma < 0.8 \\ A''\exp(\beta\sigma) & \alpha\sigma > 1.2 \\ A\left[\sinh(\alpha\sigma)\right]^n & \text{for all } \sigma \end{cases} \tag{2}$$

where $\dot{\varepsilon}$ is the strain rate, s^{-1}; R the molar gas constant, 8.314 J/(mol·K); T the thermodynamic temperature, K; Q the activation energy, kJ/mol; σ the flow stress for a given strain, MPa; and A, A', A'', α, β, n, and n' the material constants ($\alpha \approx \beta/n'$). The stress multiplier (α) is an adjustable constant that brings $\alpha\sigma$ into the correct range, giving the linear and parallel lines in plots of $\ln\dot{\varepsilon}$ vs. $\ln[\sinh(\alpha\sigma)]$ [22]. To determine these constants, the stress-strain data were used.

In these equations, the characteristic stresses, such as steady-state or peak stress, may be used [23-24]. The peak stress is more important for the industrial processes,

and the steady-state stress may not be obtained precisely, which is based on the peak stress [14, 22].

3.3. Determination of material constants for the constitutive equation

To obtain the constants of β, n, and n' at the peak stress (σ_P), $f(\sigma)$ from Eq. (2) is substituted in Eq. (1). Taking the natural logarithm on both sides, it gives the following equations.

$$\ln\dot{\varepsilon} + \frac{Q}{RT} = \ln A' + n'\ln\sigma_P \tag{3}$$

$$\ln\dot{\varepsilon} + \frac{Q}{RT} = \ln A'' + \beta\sigma_P \tag{4}$$

$$\ln\dot{\varepsilon} + \frac{Q}{RT} = \ln A + n\ln[\sinh(\alpha\sigma_P)]. \tag{5}$$

The values of β and n' can be obtained from the slope of lines in $\ln\dot{\varepsilon}-\ln\sigma_P$ and $\ln\dot{\varepsilon}-\sigma_P$ for different deformation temperatures, respectively. These are shown in Figs. 2(a) and (b). The average values of β and n' are found to be 6.025 and 0.0534 MPa^{-1}, respectively. Then, α can be calculated as $\alpha \approx \beta/n' = 0.0089$ MPa^{-1}. By obtaining the slope of lines in the plot of $\ln\dot{\varepsilon}$ vs. $\ln[\sinh(\alpha\sigma_P)]$ for different deformation temperatures in Fig. 2(c), the value of n (n=4.533) can be determined.

3.4. Calculation of the activation energy

The activation energy of deformation can be determined by the partial differential of Eqs. (3)-(5) at a constant strain rate, which yields as the following equations.

$$Q = Rn'\left[\frac{\partial\ln\sigma_P}{\partial(1/T)}\right]_{\dot{\varepsilon}} \tag{6}$$

$$Q = R\beta\left[\frac{\partial\sigma_P}{\partial(1/T)}\right]_{\dot{\varepsilon}} \tag{7}$$

$$Q = Rn\left\{\frac{\partial\ln[\sinh(\alpha\sigma_P)]}{\partial(1/T)}\right\}_{\dot{\varepsilon}} \tag{8}$$

According to the slopes of Eqs. (6)-(8) ($\ln\sigma_P$, σ_P, and $\ln[\sinh(\alpha\sigma_P)]$ vs. $1/T$), the value of Q can be obtained. These plots are shown in Fig. 3. The average values of activation energy were obtained as 435.1, 434.25, and 433.343 kJ/mol from Eqs. (6)-(8), respectively. There is not a significant difference between these values, but by analyzing the correlation coefficient (R^2), it can be understood that Eq. (8) has a better fit to the experimental data. Thus, the activation energy of AISI 321 austenitic stainless steel is equal to 433.343 kJ/mol, which is the same for other austenitic stainless steels and is considered as a reasonable estimation [22].

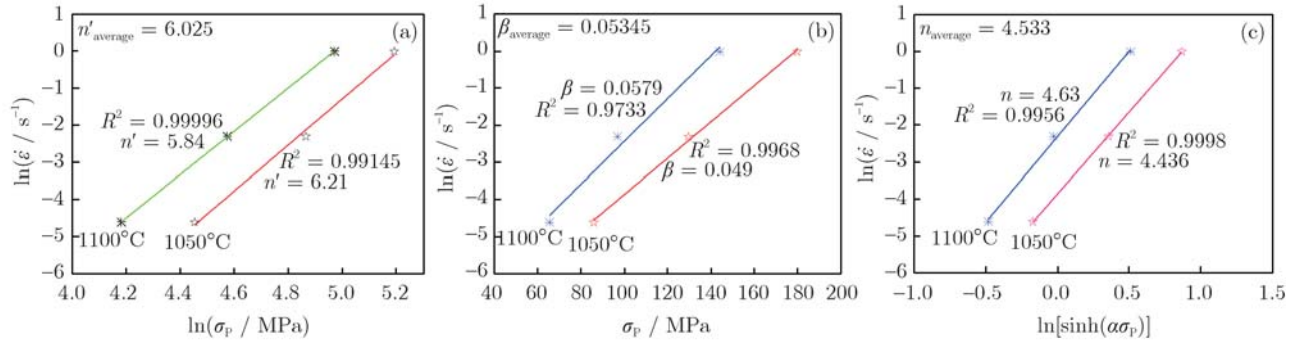

Fig. 2. Plots for determination of material constants: (a) $\ln\dot{\varepsilon}$ vs. $\ln\sigma_P$; (b) $\ln\dot{\varepsilon}$ vs. σ_P; (c) $\ln\dot{\varepsilon}$ vs. $\ln[\sinh(\alpha\sigma_P)]$.

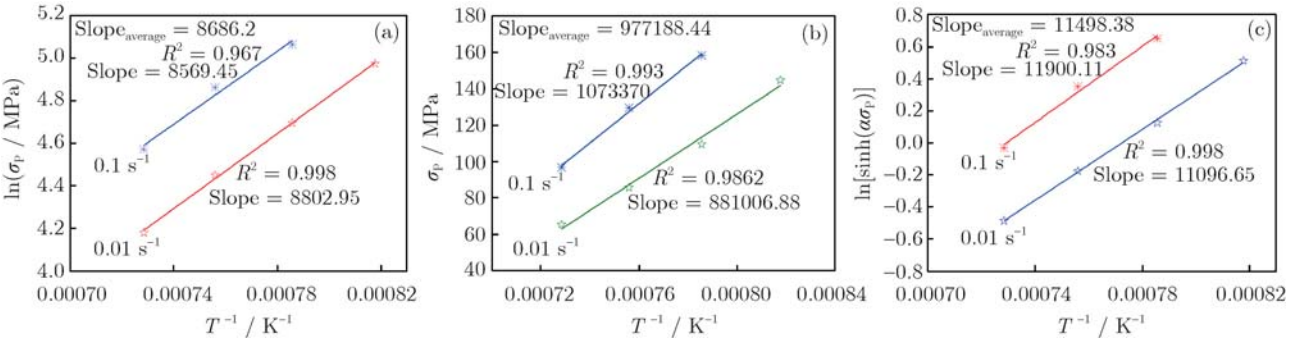

Fig. 3. Slopes of Eqs. (6)-(8): (a) $\ln\sigma_P$ vs. $1/T$; (b) σ_P vs. $1/T$; (c) $\ln[\sinh(\alpha\sigma_P)]$ vs. $1/T$.

3.5. Relationship between Zener-Hollomon parameter and peak stress

According to the deformation conditions and Eq. (1), Zener-Hollomon parameter (Z) can be estimated by Eq. (2). The relationship between Z and σ_P is determined as the following equations.

$$Z = \dot{\varepsilon}\exp\left(\frac{433.34\times10^3}{RT}\right) = 3677.54\sigma_P^{5.99} \tag{9}$$

$$Z = \dot{\varepsilon}\exp\left(\frac{433.34\times10^3}{RT}\right) = 1.49\times10^{13}\exp\left(0.0523\sigma_{\mathrm{P}}\right) \tag{10}$$

$$Z = \dot{\varepsilon}\exp\left(\frac{433.34\times10^3}{RT}\right) = 3.01\times10^{15}\left[\sinh\left(0.0089\sigma_{\mathrm{P}}\right)\right]^{4.5} \tag{11}$$

By obtaining the linear regression equations and analyzing the correlation coefficient values, it is revealed that Eq. (11) is appropriate to express the constitutive equation of AISI 321 stainless steel because of its highest correlation coefficient value. According to Eq. (11), the values of A and n are found to be 3.01×10^{15} and 4.5, respectively. Therefore, over the temperature range of 950-1100°C, the hot deformation equation of AISI 321 stainless steel can be expressed as

$$\dot{\varepsilon} = 3.01\times10^{15}\exp\left(-\frac{433.34\times10^3}{RT}\right)\left[\sinh\left(0.0089\sigma_{\mathrm{P}}\right)\right]^{4.5} \tag{12}$$

3.6. Microstructural observations

Microstructures depicted in Fig. 4 are related to specimens subjected to the different hot deformation conditions. The black particles are precipitates that remain undissolved during the reheating process. At all hot deformation conditions, DRX occurs and DRX grains become finer as the strain rate increases. This is mainly because the grains have less time to grow up at higher strain rates. Although DRX partially occurs at 1050°C and the strain rate of 1 s^{-1}, it is clearly seen that many austenite grains are elongated. Also, there are no precipitated particles on grain boundaries at the temperatures of 1050 and 1100°C and the strain rates of 0.01 and 1 s^{-1}.

In Fig. 5, the microstructures are obtained from the specimen deformed at 950°C and 0.01 s^{-1}. As seen in Fig. 5(a), the grains are elongated and perpendicular to the compression direction. Compared with Fig. 4, because of the lowest temperature and strain rate, wavy and serrated boundaries are observed, and the microstructural feature of DRX in the early stages, which is similar to the necklace structure in Fig. 5(b), has occurred. Microstructures in Figs. 5(c) and (d) are interesting. Separate and circle-like precipitates seem to be partially formed along high angle grain boundaries (HAGBs). Fig. 6 shows the SEM observations of these precipitates. Momeni *et al.* [18] have been reported the similar behavior in a superaustenitic stainless steel due to the high volume fraction of particles at 900 and 950°C. According to their approach, the presence of such precipitates can lead to DRX by applying Zener pinning force on grain boundaries.

Fig. 7 presents the energy-dispersive X-ray (EDX) spectrum taken from circle-like precipitates formed at grain boundaries. The results prove that the precipitates are complex carbides of Cr, Fe, Mn, Ni, and Ti.

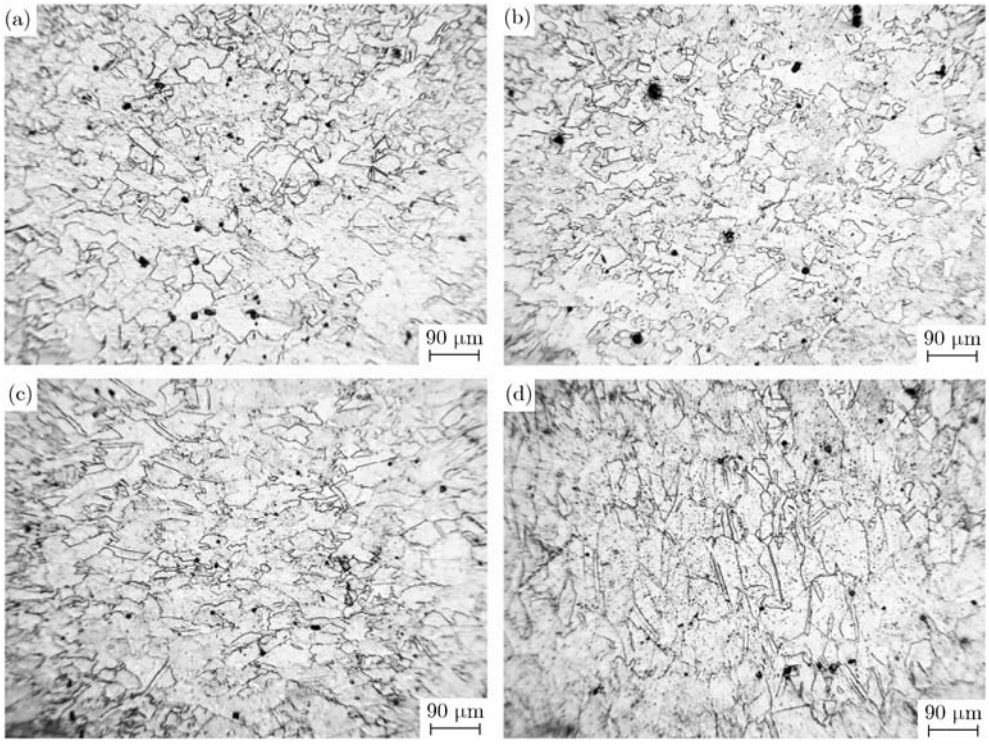

Fig. 4. Microstructures of hot deformed samples of AISI 321 stainless steel: (a) 1100°C, 0.01 s^{-1}; (b) 1050°C, 0.01 s^{-1}; (c) 1100°C, 1 s^{-1}; and (d) 1050°C, 1 s^{-1}.

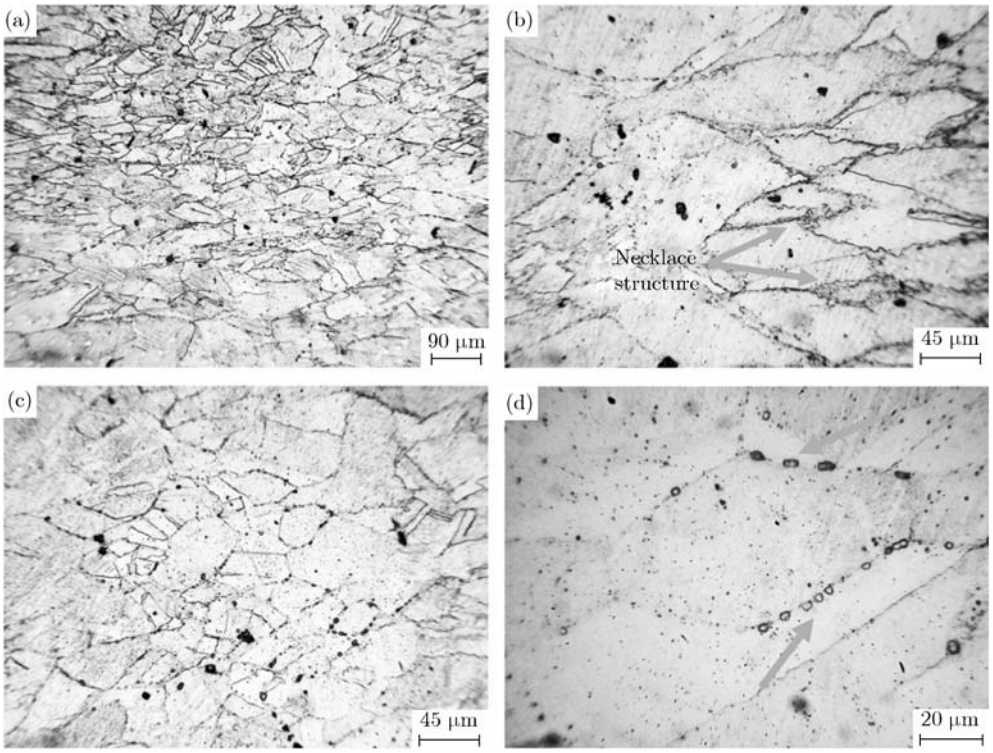

Fig. 5. Microstructures of a hot deformed sample at 950°C and 0.01 s^{-1}.

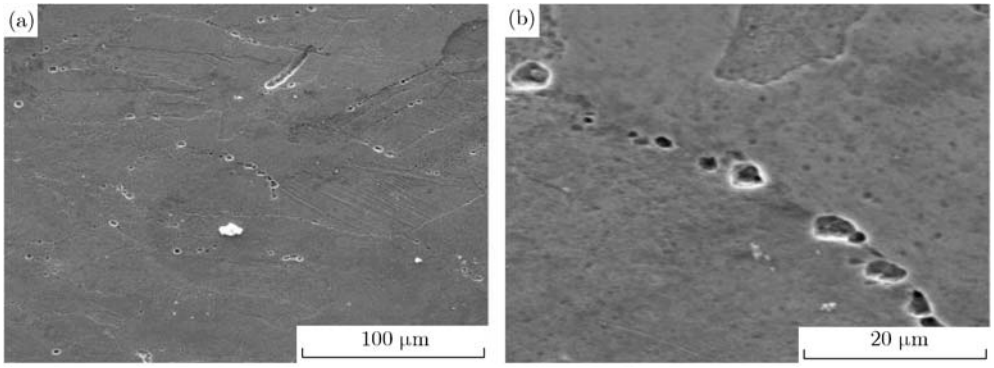

Fig. 6. Microstructures of a hot deformed sample along HAGBs at 950°C and 0.01 s^{-1}.

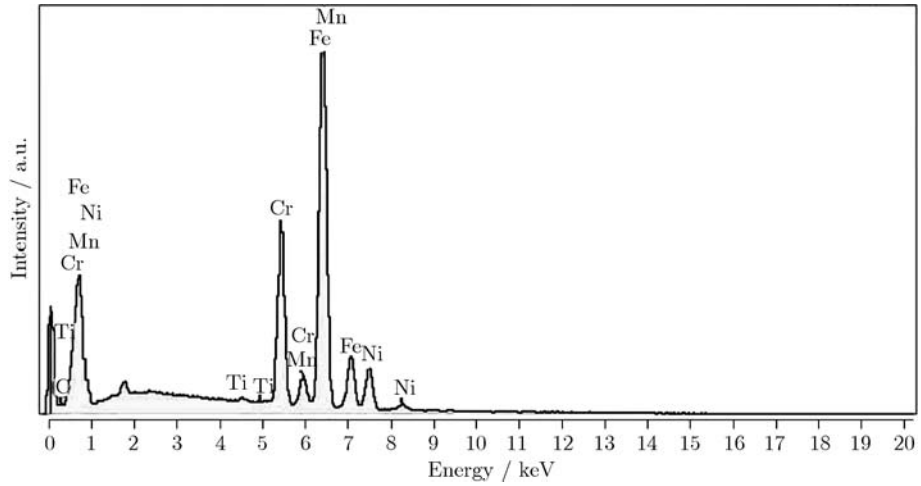

Fig. 7. EDX spectrum of the circle-like precipitates observed at grain boundaries.

4. Conclusions

(1) For AISI 321 stainless steel, the hyperbolic sine equation can be appropriate for the calculation of activation energy due to its high correlation coefficient (R^2).

(2) The hot deformation activation energy of AISI 321 stainless steel is estimated to be 433.343 kJ/mol and the hot deformation equation is established as

$$\dot{\varepsilon} = 3.01 \times 10^{15} \exp\left(-\frac{433.34 \times 10^3}{RT}\right) [\sinh(0.0089\sigma_{\mathrm{P}})]^{4.5}.$$

(3) The microstructures of the steel are affected by deformation conditions. It is shown that, at the temperature of 950°C and the low strain rate of 0.01 s^{-1}, the time for precipitation partially along grain boundaries is sufficient. However, at higher temperatures and strain rates, there is no sign of precipitation at grain boundaries.

(4) EDX microanalyses show that the circle-like precipitates are complex carbides of Cr, Fe, Mn, Ni, and Ti.

Acknowledgements

The authors gratefully acknowledged the research center of Isfahan Alloy Steel Complex (IASC) for the experimental and financial support of this work.

References

[1] D. Peckner and I.M. Bernstein, *Handbook of Stainless Steels*, McGraw-Hill, New York, 1977, p. 48.

[2] M. Chabaud-Reytier, L. Allais, C. Caes, P. Dubuisson, and A. Pineau, Mechanisms of stress relief cracking in titanium stabilised austenitic stainless steel, *J. Nucl. Mater.,* 323(2003), p. 123.

[3] K.S. Min, K.J. Kim, and S.W. Nam, Investigation of the effect of the types and densities of grain boundary carbides on grain boundary cavitation resistance of AISI 321 stainless steel under creep-fatigue interaction, *J. Alloys Compd.,* 370(2004), p. 223.

[4] K.S. Guan, X.D. Xu, Y.Y. Zhang, and Z.W. Wang, Cracks and precipitate phases in 321 stainless steel weld of flue gas pipe, *Eng. Failure Anal.,* 12(2005), p. 623.

[5] A. Pardo, M.C. Merino, A.E. Coy, F. Viejo, M. Carboneras, and R. Arrabal, Influence of Ti, C and N concentration on the intergranular corrosion behaviour of AISI 316Ti and 321 stainless steels, *Acta Mater.,* 55(2007), p. 2239.

[6] W.H. Zhang, J.L. Wu, Y.H. Wen, J.J. Ye, and N. Li, Characterization of different work hardening behavior in AISI 321 stainless steel and hadfield steel, *J. Mater. Sci.,* 45(2010), p. 3433.

[7] K.S. Guan, X.D. Xu, H. Xu, and Z.W. Wang, Effect of aging at 700°C on precipitation and toughness of AISI 321 and AISI 347 austenitic stainless steel welds, *Nucl. Eng. Des.*, 235(2005), p. 2485.

[8] R.C. de Sousa, J.C. Cardoso Filho, A.A. Tanaka, A.C.S. de Oliveira, and W.E.I. Ferreira, Effects of solution heat treatment on grain growth and degree of sensitization of AISI 321 austenitic stainless steel, *J. Mater. Sci.,* 41(2006), No. 8, p. 2381.

[9] V. Moura, A.Y. Kina, S.S.M. Tavares, L.D. Lima, and F.B. Mainier, Influence of stabilization heat treatments on microstructure, hardness and intergranular corrosion resistance of the AISI 321 stainless steel, *J. Mater. Sci.,* 43(2008), p. 536.

[10] K.D. Nair, Structure and strength during hot working of an austenitic steel, *Metallography,* 4(1971), p. 375.

[11] L. Havela, P. Kratochvíl, P. Lukáč, B. Smola, and A. Svobodová, Softening during and after the hot deformation of the AISI 321 steel with respect to practical applications, *Czech. J. Phys. B,* 38(1988), p. 384.

[12] E.I. Poliak and J.J. Jonas, Initiation of dynamic recrystallization in constant strain rate hot deformation, *ISIJ Int.,* 43(2003), No. 5, p. 684.

[13] R. Herbertz and H. Wiegels, A method of performing the frictionless cylinder upsetting test for plotting stress-strain curves, *Stahl Eisen.*, 101(1981), p. 89.

[14] H. Mirzadeh, A. Najafizadeh, and M. Moazeny, Flow curve analysis of 17-4 PH stainless steel under hot compression test, *Metall. Mater. Trans. A,* 40(2009), p. 2950.

[15] R. Ebrahimi and A. Najafizadeh, A new method for evaluation of friction in bulk metal forming, *J. Mater. Process. Technol.*, 152(2004), p. 136.

[16] H. Mirzadeh and A. Najafizadeh, Extrapolation of flow curves at hot working conditions, *Mater. Sci. Eng. A*, 527(2010), No. 7-8, p. 1856.

[17] A. Najafizadeh and J.J. Jonas, Predicting the critical stress for initiation of dynamic recrystallization, *ISIJ Int.,* 46(2006), No. 11, p. 1679.

[18] A. Momeni, K. Dehghani, H. Keshmiri, and G.R. Ebrahimi, Hot deformation behavior and microstructural evolution of a superaustenitic stainless steel, *Mater. Sci. Eng. A*, 527(2010), p. 1605.

[19] D.N. Zou, Y. Han, D.N. Yan, D. Wang, W. Zhang, and G.W. Fan, Hot workability of 00Cr13Ni5Mo2 supermartensitic stainless steel, *Mater. Des.*, 32(2011), p. 4443.

[20] C. Zener and J.H. Hollom, Effect of strain rate upon plastic flow of steel, *J. Appl. Phys.*, 15(1944), p. 22.

[21] A. Cingara and H.J. McQueen, New method for determining sinh constitutive constants for high temperature deformation of 300 austenitic steels, *J. Mater. Process. Technol.*, 36(1992), p. 17.

[22] H.J. McQueen and N.D. Ryan, Constitutive analysis in hot working, *Mater. Sci. Eng. A,* 322(2002), p. 43.

[23] Y.C. Lin, M.S. Chen, and J. Zhong, Constitutive modeling for elevated temperature flow behavior of 42CrMo steel, *Comput. Mater. Sci.,* 42(2008), p. 470.

[24] S. Mandal, V. Rakesh, P.V. Sivaprasad, S. Venugopal, and K.V. Kasiviswanathan, Constitutive equations to predict high temperature flow stress in a Ti-modified austenitic stainless steel, *Mater. Sci. Eng. A,* 500(2009), p. 114.